Heat transfer behaviour of supercritical nitrogen in the large specific heat region flowing in a vertical tube

Negoescu, Ciprian; Li, Yongliang; Al-Duri, Bushra; Ding, Yulong

DOI:
10.1016/j.energy.2017.04.047

Document Version
Peer reviewed version

Citation for published version (Harvard):
Negoescu, C, Li, Y, Al-Duri, B & Ding, Y 2017, 'Heat transfer behaviour of supercritical nitrogen in the large specific heat region flowing in a vertical tube', *Energy*, vol. 134, pp. 1096-1106.
https://doi.org/10.1016/j.energy.2017.04.047

Heat transfer behaviour of supercritical nitrogen in the large specific heat region flowing in a vertical tube

Ciprian Constantin Negoescu, Yongliang Li*, Bushra Al-Duri, Yulong Ding
School of Chemical Engineering, University of Birmingham
Edgbaston B15 2TT, Birmingham, United Kingdom
* Corresponding author. Email: y.li.1@bham.ac.uk; Tel: +44 (0) 121 414 5135

Abstract: This work investigates the heat transfer behaviour of supercritical nitrogen (SCN) for the ultimate goal of optimal design of cryogenic processes/systems. To this end, a comprehensive numerical study was carried out to evaluate the heat transfer coefficient for SCN flowing in a test section under representative conditions. This paper presents the results for nitrogen flowing vertically upward in a 2 mm diameter smooth tube. CFD simulations were conducted at two supercritical pressures (3.5 and 7 MPa) for low and high mass flux at different heat to mass flux ratios (q/G). The objective is to develop reliable prediction approaches regarding the heat transfer coefficient (HTC) in the large specific heat region using the commercially available CFD software Fluent by employing the *k*-*ε* turbulence model with enhanced wall treatment. The effects of relevant parameters such as mass flux and heat flux on heat transfer performance, and the influence of operating pressure are discussed. For example, while the working pressure is close to the critical value, i.e. 3.5 MPa, the high specific heat capacity at pseudo-critical temperature produces a peak in the heat transfer coefficient trend. On the other hand, when the pressure increases to 7 MPa the heat transfer behaviour changes due to the smooth variation of thermophysical properties and as a result the HTC trend does not show a peak even at low heat flux. It is found that the heat transfer process transfers from normal mode to deterioration mode while increasing the heat flux. Fundamentally this deterioration is caused by the variation of thermo-physical properties under high mass flux conditions and by the buoyancy forces for low flow rate.

Keywords: supercritical nitrogen, heat transfer, large specific heat region, waste cold recovery

1. Introduction

A fluid is called supercritical when it reaches a temperature and pressure above its critical point (P_c, T_c), where distinction between liquid and gas phases no longer exists. Supercritical fluids possess unique thermodynamic properties that are significantly different from their subcritical states leading to different behavioural profiles and opening up a wide range of applications especially in the domains of energy production, environment protection and green processes [1–6]. They become green solvents for extraction, particle production and superior reaction media for a wide range of catalytic and non-catalytic reactions. In energy related aspects, supercritical water is actively being studied for the use in new generation nuclear power stations to enhance the efficiency [7]. Supercritical CO_2 has also gained research interests as a working fluid in the supercritical Rankine cycle with applications regarding low-grade heat conversion, offering system compactness and environmental safety among advantages [8].

Supercritical nitrogen/air is also attracting attention with the new developed cryogenic industry. For example in Liquid Air Energy Storage (LAES) which uses liquid air/nitrogen as both energy storage carrier and heat transfer fluid [9,10], the heat transfer performance of the supercritical flow is key to achieve a reasonable system round-trip efficiency [11]. Furthermore, supercritical nitrogen/air also plays a key role in recycling waste cold from the Liquefied Natural Gas (LNG) regasification process. In conventional terminals, LNG is normally warmed by seawater or burning some of the natural gas, and the cold given off by evaporation is wasted [12]. However, if superficial nitrogen/air rather than seawater/gas is used to warm the LNG, the resulting supercritical cold nitrogen/air can be fed into an air/nitrogen liquefier to dramatically decrease the electricity consumption (potentially two thirds less than a conventional unit) of LAES or air liquefaction/separation [10]. In LAES or LNG cold recovery processes, the working fluid air/nitrogen transfers from subcritical to supercritical state, where its thermodynamic properties change dramatically

with temperature and pressure creating important effects on system behaviour. While the heat exchanger design for common applications is more or less straightforward, heat transfer analysis in supercritical fluids is more challenging mainly because the thermo-physical properties of the fluids vary strongly near the pseudo-critical temperature [13]. Such variations lead to strong variations of the heat transfer coefficient (h) which in turn influences the overall heat transfer coefficient (U) and implicitly the heat exchange surface area (A). Thus, the optimal design of heat exchangers, which can operate efficiently under both subcritical and supercritical conditions, is rather complicated even more so because the Nusselt number correlations for heat transfer in supercritical fluids are valid only in limited cases.

The strong variation of physical properties of nitrogen (critical pressure P_c = 3.4 MPa, critical temperature T_c = 126.2 K) becomes evident when plotted as a function of temperature at constant pressures. Fig. 1 (a) and (b) show the variation of density, specific heat capacity, thermal conductivity, and viscosity. It can be seen that at 3.5 MPa for a very narrow temperature range ($\Delta T \approx 3$ K), the density and dynamic viscosity undergo a significant drop while the thermal conductivity and specific heat experience a sharp increase. Consequently, the temperature interval with important change in c_p is known as the *large specific heat region*. At each pressure where there is a maximum value of the specific heat, the corresponding temperature is called the "pseudo-critical" temperature T_{pc}. In contrast, the variations are less dramatic at 7 MPa where the properties transition smoothly as temperature increases.

In general the heat transfer process falls under one or a combination of the following modes: normal heat transfer, deteriorated heat transfer (HTD), and enhanced heat transfer (HTE) [14]. Many studies have been published in the past decades presenting heat transfer results at supercritical conditions for various fluids (water, CO_2, organic compounds, helium, etc.) with only a few focused on nitrogen [15–22]. In the early 1970's Yamagata et al. investigated the heat transfer of supercritical water flowing in horizontal and vertical tube geometries [23]. They showed that at low heat fluxes, the heat transfer was enhanced near the pseudo-critical temperature while heat transfer deterioration occurred at high heat fluxes. Referring to Yamagata's experimental results, Kim et al. performed a CFD study in which they concluded that the *k-ε* model with enhanced wall treatment provides a reliable way to predict the heat transfer characteristics in supercritical water flowing vertically upward [24]. In addition, Lei et al. and Zhang et al. followed Yamagata's study and recommend that for horizontal flows *k-ε* turbulence model and its variations is also quite reliable, offering at least a qualitative description of the heat transfer process at supercritical conditions [25,26]. Li et al. highlighted the effect of heat flux and buoyancy with heat transfer experiments in supercritical CO_2 and they concluded that the complex wall temperature profile obtained at high heat flux gave rise to deterioration followed by recovery [27]. Zhang et al. also reported an experimental study on heat transfer in supercritical nitrogen flowing in a vertical tube [22]. Similar to above cases the variation of thermo-physical properties and buoyancy had a significant contribution to system performance deterioration. However in their simulations the authors did not discuss in detail the heat transfer coefficient in the large specific heat region. Therefore in this work we will investigate the heat transfer behavior of nitrogen using the *k-ε* turbulence model and the aim is to obtain primarily a qualitative description of the heat transfer coefficient in the large specific heat region at various working conditions taking into account the influence of buoyancy and flow acceleration. This study represents one of the steps necessary for the optimal design of heat exchangers in LAES and waste cold recovery.

2. Methodology

2.1. Numerical approach

The standard *k-ε* model employed in the present analysis is one of the most popular RANS turbulence models and was developed in the early 1970's [28]. The pressure based solver used in this work computes the governing equations for continuity, momentum, energy and transport of *k* and *ε* in a segregated manner which improves the memory demand. More details on the governing equations and implementation of the *k-ε* turbulence model can be found in the ANSYS Fluent theory guide [29].

2.2. Turbulence model validation

In order to gain confidence in the selected turbulence model a number of experimental cases found after a comprehensive literature survey were simulated first. These calculations refer to supercritical nitrogen, supercritical carbon dioxide, and supercritical water and the cases were chosen based on the condition that the experimental results should cover the large specific heat region. Moreover, the simulated cases include low and high mass flux conditions as well as low and high heat flux. In the cases of nitrogen and carbon dioxide the maximum absolute error between experiments and numerical results was about 5%, while for water the maximum was 15%.

The model validation study was performed in 3D space, steady state, and the results are presented similarly to the original experimental data.

It is important to point out that the geometry should be meshed according to the working parameters. Also, for increased accuracy the grid close to the wall should be carefully meshed based on the non-dimensional distance y^+. Hence, the grid resolution near the wall needs to be sufficiently high such that the boundary layer is resolved. Following these requirements, with the imposed mass flux and density, the inlet velocity is calculated. The Reynolds number is then computed from velocity, density, tube diameter and dynamic viscosity. The resulting Re serves two purposes: i) determine the entrance region length to ensure a fully developed flow ii) calculate the friction coefficient. Further calculations based on the flat-plate boundary layer theory are carried out in order to determine the first cell layer distance from the wall.

In the present setup a y^+ value less than 1 for the highest Re number was used to generate a mesh which could capture the effect of the sharp variation of thermo-physical properties. Therefore, the mesh cells adjacent to the wall had the minimum height.

Using the k-ε turbulence model with enhanced wall treatment, the boundary conditions for domain inlet and outlet were set as velocity inlet and pressure outlet, respectively, while the wall was constant heat flux boundary condition.

The least squares cell based scheme was adopted for the spatial discretization of gradients, while the momentum, turbulent kinetic energy, turbulent dissipation rate, and energy employed the second order upwind scheme. The model equations were solved sequentially by the segregated pressure based solver with SIMPLE scheme for pressure-velocity coupling. As the Mach number was less than 0.3, the fluids were assumed incompressible. The convergence of the numerical solution was evaluated by carefully monitoring the scaled residuals, convergence criterion 10^{-6}, and the variation of wall and bulk temperatures as well. For each fluid the thermo-physical properties were obtained from the NIST Standard Reference Database 23 (REFPROP) Version 8.0 [30] and the variation as a function of temperature was written in C language with which a shared dynamic library was created by compiling the code through Fluent's interface.

Nitrogen

Shown in Fig. 2 are the experimental results presented by Zhang et al. [22] compared to the numerical validation. In their study the authors investigated the heat transfer of supercritical nitrogen flowing vertically upward in a 2 mm diameter tube and 220 mm in length, at various working conditions. During experiments the pressure was kept constant at 3.6 MPa and the heat transfer performance was assessed for a number of cases. To prove the validity of the k-ε turbulence model applied to flow and heat transfer problems in fluids in supercritical state three experimental cases were simulated.

As it can be seen from Fig. 2 a good overall agreement is obtained when the simulations are performed under the same conditions as in experiments. The most consistent numeric predictions of the wall temperature were obtained when the inlet temperature was 132.2 K at 10527 W/m^2 heat flux.

Carbon dioxide

The model was also validated with supercritical CO_2 data obtained through experiments by Kim et al. [31].

In their setup carbon dioxide with an inlet temperature of 302.15 K flowing downward entered a vertical tube (D=4.5 mm) under constant heat flux. The fluid was heated trans-critically at three pressures, 7.437 MPa (Fig. 3 (a)), 8.196 MPa (Fig. 3 (b)), and 8.8 MPa (Fig. 3 (c)).

It can be seen in Fig. 3 that while the bulk temperature is in very good agreement, the wall temperature comparison shows a small but noticeable discrepancy. The values are slightly over-predicted by the model in all cases although the maximum overall absolute found is about 5%. Taking into consideration the mostly qualitative nature of this numerical study the model is considered valid in these conditions.

Water

To further verify the validity of the turbulence model, an experimental case of heat transfer in supercritical water described by Yamagata et al. [23] was analysed numerically with water flowing vertically upward at a pressure of 24.5 MPa. The 7.5 mm diameter tube was heated by a 233000 W/m^2 heat flux. The comparison between simulation and experiment displayed in Fig. 4 reveals a good performance of the *k-ε* model. As shown, the heat transfer coefficient increases very fast when the bulk temperature approaches T_{pc} where the specific heat reaches its maximum. After this point is crossed all thermo-physical properties drop, as a result the wall temperature increases to provide the higher driving force needed to overcome the heat transfer resistance thus satisfying the energy equation.

2.3. Numerical method and boundary conditions

The total length of the computational domain (Fig. 5) was 1560 mm and 560 mm, respectively, from which the first 60 mm represent the developing section to ensure a fully developed state of nitrogen flow. Cases with low heat flux conditions were run for a tube length of 1560 mm while the tube length was decreased to 560 mm to prevent the wall temperature exceeding 460 K at high heat flux, while other simulation parameters are listed in Table 1.

The following results were obtained with the simulation setup described in the model validation section. As such, all simulations were carried out in 3D space, steady state, using the *k-ε* turbulence model with enhanced wall treatment. When applied to fine grids this option makes it possible to fully resolve the laminar sublayer where the high Reynolds flow changes to laminar. Without the high mesh resolution the modelled transport properties would be overestimated resulting in a lower wall temperature.

Regarding the solver setup, spatial discretization, boundary conditions, solution convergence, and user defined functions implementing the variation of thermo-physical properties an identical methodology was adopted as explained above.

2.4. Grid independence study

When dealing with a numerical analysis using CFD tools the solution convergence for only one mesh size is not enough to draw meaningful conclusions about the specific problem investigated. In especially tough conditions such is the case with flow and heat transfer in supercritical fluids the accuracy is greatly influenced by the mesh quality, cell count and the presence of inflation layers. Hence, it is necessary that a grid independence study is performed. For this purpose the same simulation conditions were applied on four structured non-uniform meshes of different sizes and the outcomes were compared.

The geometry used in the grid independence study was the 3D tube with inside diameter D= 2 mm and length 1560 mm which had nitrogen flowing at 3.5 MPa, mass flux 1200 kg/m^{2}s and heat flux 120000 W/m^{2}K. Regarding the boundary layer and mesh generation, the first cell layer from the wall was calculated with a non-dimensional wall distance $y^+ = 0.4$ in all cases and enlarged toward the tube centre by a growth factor of 1.2. The resulting initial mesh (M1) 37 × 32 × 390 (radial × circumferential × axial) had a cell count of approximately 400 000. The other three were generated by doubling the cell density of the previous

one giving 800 000 (M2), 1 600 000 (M3), and 3 200 000 (M4), respectively. A detailed view of the inlet and boundary layer mesh in the axial direction is presented in Fig. 6.

Shown in Fig. 7 is the comparison between the average wall temperatures obtained with the four grids. After the residuals dropped to the desired value and the imbalances were below 1 % the case with mesh M1 converged with a resulting average wall temperature of 206.35 K. Increasing the grid resolution to 800 000 control volumes the average wall temperature was 206.62 K. For the remaining two grids the variable of interest had the values 207.35 K and 207.58 K, respectively. The numerical predictions in the following section were completed using the third mesh (M3) settings because it satisfied a set tolerance of ±0.5 K while providing a good balance between accuracy and computational time.

3. Results and discussions

The heat transfer coefficient (HTC) was calculated from the imposed constant heat flux divided by the simulation values of the inner wall and bulk temperature (Eq. 1).

$$h(x) = \frac{q_w}{T_w(x) - T_b(x)} \quad \text{(Eq. 1)}$$

In order to evaluate the heat transfer mode, a reference heat transfer coefficient h_0 was calculated and compared to the heat transfer coefficient h evaluated from simulations. In this work h_0 was obtained from the Dittus-Boelter correlation (Eq. 2), which is suitable for single phase flows at subcritical conditions and generally provides good results away from the pseudo-critical temperature [32].

$$Nu_b = \frac{h_0 D}{\lambda_b} = 0.023 Re_b^{0.8} Pr_b^{0.4} \quad \text{(Eq. 2)}$$

It was found that heat transfer deterioration (HTD) occurs when the ratio $h/h_0 < 0.3$, heat transfer enhancement (HTE) occurs when $h/h_0 > 1$, and normal heat transfer when $0.3 < h/h_0 < 1$ [33]. Therefore in order to capture the relevant variations, the mass and heat flux were swept over a wide range of values in the present simulation study and only a selection of cases, those which can reflect the variations, were discussed in the following.

The simulation results for heat transfer in supercritical nitrogen are presented in terms of h and reference h_0 plotted against bulk temperature and tube length. On each graph the dashed vertical lines refer to the pseudo-critical temperature while the horizontal one represents the threshold for deterioration as defined above.

The main difference between investigations carried out at low and high mass fluxes is how the system performance is affected by the heat flux, namely the mechanism by which heat transfer deterioration occurs.

When the mass flux is low and heat flux high, the turbulence is suppressed because the strong buoyancy force leads to a flat velocity profile near the wall. With suppressed turbulence the energy transport capability of the system is also reduced. However, if the heat flux is sufficiently low so that buoyancy effects disappear heat transfer enhancement can be achieved instead. This behaviour is triggered by the ability of the increased specific heat to carry more energy from the wall into the bulk.

In cases of intense heating at high mass fluxes, the drop in thermo-physical values creates a localized increase of wall temperature. The temperature difference between wall and bulk increases and the HTC is reduced [34]. For example, considering the tube geometry with a wall temperature around T_{pc} the fluid is stratified in the radial direction by sharp thermo-physical gradients. In this layered configuration the bulk properties are very different from the near wall region. In the boundary layer the density and thermal conductivity decrease steeply in such a way that the zone where the heat transfer resistance becomes concentrated acts as insulation.

On the other hand, high flow rates can overcome the effects of density variation close to the tube wall, thus diminishing the buoyancy effects which can lead to deterioration. Moreover, at low heat flux the

HTC value is proportional to the flow rate; hence, the heat transfer coefficient has higher values at high mass flux.

3.1. Low mass flux

It is well known that the heat transfer in fluids at supercritical conditions is influenced by parameters such as mass flux, heat flux and pressure. In this section the simulation results obtained for a low mass flux ($G = 300$ kg/m^{2}s) are discussed.

Fig. 8 (a) - (c) show the heat transfer behaviour of supercritical nitrogen at increasing heat flux for a working pressure of 3.5 MPa. It can be seen from Fig. 8 (a) that at low heat flux conditions ($q/G = 38$), as nitrogen changes trans-critically the HTC trend sharply increases reaching a peak near the pseudo-critical temperature (126.83 K) after which, it drops significantly and continues to decrease monotonically. This peak appears when there is a minimum temperature difference between wall and bulk fluid. Owing to this effect is the high specific heat at T_{pc} that translates into the same amount of energy being transported by a relatively small difference between T_w and T_b.

As the heat flux progresses to higher values the heat transfer deteriorates, most notably for $q/G = 333$ (Fig. 8 (b)). The HTC peaks become less noticeable meaning the ΔT increases compared with low heat flux conditions. Deterioration occurs close to the tube inlet at high heat flux, however, the system recovers from deterioration and enters normal mode further away from the tube inlet where the bulk temperature is significantly higher than T_{pc} (Fig. 8 (c)).

In supercritical fluids, the peak in specific heat capacity becomes less noticeable as pressure increases. Moreover, all thermophysical properties change smoothly as a function of temperature. For comparison the specific heat capacity of nitrogen at pseudo-critical temperature ($T_{pc} = 142.5$ K) at 7 MPa is $c_p \approx 4069$ J/kgK in contrast with the 3.5 MPa case ($c_p \approx 133422$ J/kgK, $T_{pc} = 126.83$ K).

To highlight the effect of working pressure on heat transfer behaviour the simulation cases for 3.5 MPa were performed at 7 MPa. As evidenced in Fig. 9 (a) – (c) a smooth trend of the heat transfer coefficient is obtained when thermophysical properties do not experience rapid variation. Furthermore, there is no deterioration even at high heat flux. Although deterioration is not present, the heat transfer performance in the large specific heat region is substantially reduced when the ratio q/G is large.

In addition, the HTC magnitude is very similar at bulk temperatures greater than T_{pc} at both pressures investigated.

3.2. High mass flux

With an increase in mass flux and keeping constant q/G ratio an immediate effect is the growth in HTC amplitude as shown in Fig. 10 (a) compared with the 300 kg/m^{2}s case in Fig. 8 (a). The values predicted by the model show similar behaviour although a more pronounced deterioration is visible for $q/G \geq 200$ at 3.5 MPa (Fig. 10 (b)). Also, the bulk temperature at which the system recovers from deterioration is slightly higher at high mass flux than at low flow rates. Note that although the HTC trends are similar in all cases, the vertical axis scale is different such that a better visibility is achieved.

In accordance with the general behaviour of heat transfer in supercritical fluids the HTC values for 7 MPa cases at high flow rates (Fig. 11 (a)) were higher than the predictions for low mass flux (Fig. 9 (a)).

A smoother variation of physical properties exhibited at higher pressures does not guarantee that the heat transfer impairment is avoided. The system is still sensitive to decreasing density, thermal conductivity, etc. but to a lesser extent compared with the 3.5 MPa case.

Fig. 11 (b) illustrates that despite the large increase in mass flux to 1200 kg/m^{2}s deterioration occurs at the largest heat to mass flux ratio $q/G \approx 333$ ($q = 400$ kW/m^2).

3.3.Buoyancy and flow acceleration effects

When the fluid is heated and the inner wall temperature becomes much higher than T_{pc} while the bulk temperature remains smaller than or equal to T_{pc}, a significant difference in density occurs which induces a change in flow structure due to buoyancy. Below T_{pc} the fluid behaves like a liquid while above T_{pc} it has gas-like properties. In certain conditions, this phenomenon is the dominant factor in determining heat transfer performance [35]. To analyse this effect, the buoyancy parameter Bo^* is introduced by taking into consideration the Grashof, Reynold, and Prandtl numbers [36]. For vertical tubes Bo^* is expressed as:

$$Bo^* = \frac{Gr_q}{Re^{3.425}\mathrm{Pr}^{0.8}} \quad \text{(Eq. 3)}$$

Where Gr_q is the Grashof number based on wall heat flux calculated by

$$Gr_q = \frac{g\beta_b D^4 q_w}{\nu_b^2 \lambda_b} \quad \text{(Eq. 4)}$$

Jackson and Hall suggested that the heat transfer in turbulent flow is greatly influenced by buoyancy when $Bo^* > 5.6\times10^{-7}$. Hence, a combination of low mass flux with high heat flux is expected to show this kind of behaviour. Fig. 12 (a) and (b) show that buoyancy effects indeed influence the heat transfer deterioration at low mass fluxes as Bo^* is greater than 5.6×10^{-7} for $q/G \geq 100$. Not shown in the figures are the Bo^* results calculated for 1200 kg/m^{2}s where the buoyancy parameter was smaller than 5.6×10^{-7} along the tube length. This behaviour indicates that high flow rates overcome the effects induced by density variation.

Likewise, under high heat flux conditions significant thermal expansion effects can play an important role in determining system performance as well. The strong expansion of fluid gives rise to flow acceleration which can result in a relaminarization of turbulent boundary layer [37]. With impaired diffusion of momentum and energy the heat transfer capabilities decrease. To account for this behaviour McEligot et al. introduced the flow acceleration parameter K_v [22]:

$$K_v = \frac{4q_w D}{Re_b^2 \mu_b c_{p,b} T_b} \quad \text{(Eq. 5)}$$

Moretti and Kays suggested that the flow is likely to remain turbulent when $K_v < 3\times10^{-6}$, and conversely, relaminarization is probable to occur if $K_v > 3\times10^{-6}$ [38].

The flow acceleration parameter K_v was calculated for all simulation cases and it was found that the values were always lower than 3×10^{-6} in all cases, meaning that the flow acceleration is not high enough to cause flow laminarization and consequently deterioration.

4. Conclusions

This numerical study has shown that the heat transfer in supercritical nitrogen in the large specific heat region is greatly influenced by the rapid variation of thermo-physical properties. Adding to this, the heat flux and mass flux play an important role as well.

Lower values of the heat flux produce higher values of the heat transfer coefficient, while the trend shows deterioration at high heat flux. Heat transfer deterioration is caused by the variation of physical properties coupled with buoyancy effects. On the other hand, flow acceleration was not found to have an influence in the cases discussed in this study. Moreover, the values of the heat transfer coefficient in the large specific region are proportional to the mass flux such that by increasing the mass flux a positive effect on the heat transfer intensity is observed. Also, in our cases the heat transfer coefficient magnitude is proportional to the mass flux when considering the same q/G ratio.

The peak in the heat transfer coefficient trend is due to the high specific heat capacity at pseudo-critical temperature. If c_p at T_{pc} is small, this peak disappears and the curve becomes smoother as it can be seen from the 7 MPa case.

Further investigations are necessary by both experimental and numerical methods considering different tube geometries and flow orientation in order to gain additional information about the flow and heat transfer in supercritical nitrogen.

Acknowledgement

This work was supported by Air Products PLC and the UK Engineering and Physical Sciences Research Council under the grants EP/N000714/1 and EP/N021142/1.

Nomenclature

Bo^*, buoyancy parameter
c_p, isobaric specific heat capacity (J/kgK)
D, diameter (mm)
g, gravitational acceleration (m/s^2)
G, mass flux (kg/m^2s)
Gr_q, Grashof number based on wall heat flux
h, local heat transfer coefficient (W/m^2K)
h_0, reference heat transfer coefficient (W/m^2K)
K_v, acceleration parameter
Nu, Nusselt number
P, pressure (MPa)
Pr, Prandtl number
q, heat flux (W/m^2)
Re, Reynolds number
T, temperature (K)
(x), axial direction
y^+, non-dimensional wall distance

Greek symbols
β, volume expansion coefficient (1/K)
λ, thermal conductivity, (W/m K)
μ, dynamic viscosity (Pa s)
ν, kinematic viscosity (m^2/s)
ρ, density (kg/m^3)

Subscripts
b, evaluated at bulk
c, critical point
pc, pseudo-critical
w, evaluated at wall

References

[1] Williams DF. Extraction with supercritical gases. Chem Eng Sci 1981;36:1769–88. doi:10.1016/0009-2509(81)80125-X.

[2] Li Z, Wu Y, Tang G, Zhang D, Lu J. Comparison between heat transfer to supercritical water in a smooth tube and in an internally ribbed tube. Int J Heat Mass Transf 2015;84:529–41. doi:10.1016/j.ijheatmasstransfer.2015.01.047.

[3] Gouw TH, Jentoft RE. Supercritical Fluid Chromatography. J Chromatogr 1972;68:303–23. doi:10.1016/S0021-9673(00)85722-2.

[4] Liao SM, Zhao TS. An experimental investigation of convection heat transfer to supercritical carbon dioxide in miniature tubes. Int J Heat Mass Transf 2002;45:5025–34. doi:10.1016/S0017-9310(02)00206-5.

[5] Knez Ž, Markočič E, Leitgeb M, Primožič M, Knez Hrnčič M, Škerget M. Industrial applications of supercritical fluids: A review. Energy 2013;77:235–43. doi:10.1016/j.energy.2014.07.044.

[6] Campardelli R, Baldino L, Reverchon E. Supercritical fluids applications in nanomedicine. J Supercrit Fluids 2015;101:193–214. doi:10.1016/j.supflu.2015.01.030.

[7] Su Y, Chaudri KS, Tian W, Su G, Qiu S. Optimization study for thermal efficiency of supercritical water reactor nuclear power plant. Ann Nucl Energy 2014;63:541–7. doi:10.1016/j.anucene.2013.08.023.

[8] Sarkar J. Review and future trends of supercritical CO2 Rankine cycle for low-grade heat conversion. Renew Sustain Energy Rev 2015;48:434–51. doi:10.1016/j.rser.2015.04.039.

[9] Akhurst M, Atkins A, Uk R, Bruges R, Cooper S, Consulting S, et al. Liquid Air in the energy and transport systems. The Centre for Low Carbon Futures; 2013.

[10] Radcliffe J, Williams RA. Liquid Air Technologies – a guide to the potential. 2013.

[11] Ding Y, Tong L, Zhang P, Li Y, Radcliffe J, Wang L. Chapter 9 – Liquid Air Energy Storage. Elsevier Inc.; 2016. doi:10.1016/B978-0-12-803440-8.00009-9.

[12] Stougie L, Kooi HJ Van Der. Exergy Efficient Application of LNG Cold. In: Favrat D, Maréchal F, editors. 23rd Int. Conf. Effic. Cost, Optim. Simulation, Environ. Impact Energy Syst., vol. II, Lausanne: ECOS; 2010, p. 14–7.

[13] Cheng X, Schulenberg T. Heat Transfer at Supercritical Pressures - Literature Review and Application to an HPLWR. vol. 6609. Karlsruhe: 2001.

[14] Mokry S, Pioro I, Farah A, King K, Gupta S, Peiman W, et al. Development of supercritical water heat-transfer correlation for vertical bare tubes. Nucl Eng Des 2011;241:1126–36. doi:10.1016/j.nucengdes.2010.06.012.

[15] Brunner G. Supercritical process technology related to energy and future directions – An introduction. J Supercrit Fluids 2015;96:11–20. doi:10.1016/j.supflu.2014.09.008.

[16] Hu L, Chen D, Huang Y, Li L, Cao Y, Yuan D, et al. Investigation on the performance of the supercritical Brayton cycle with CO2-based binary mixture as working fluid for an energy transportation system of a nuclear reactor. Energy 2015;89:874–86. doi:10.1016/j.energy.2015.06.029.

[17] Serrano IP, Linares JI, Cantizano a., Moratilla BY. Enhanced arrangement for recuperators in supercritical CO2 Brayton power cycle for energy conversion in fusion reactors. Fusion Eng Des 2014;89:1909–12. doi:10.1016/j.fusengdes.2014.03.083.

[18] Pioro IL, Khartabil HF, Duffey RB. Heat transfer to supercritical fluids flowing in channels - Empirical correlations (survey). Nucl Eng Des 2004;230:69–91. doi:10.1016/j.nucengdes.2003.10.010.

[19] Ahn Y, Bae SJ, Kim M, Cho SK, Baik S, Lee JI, et al. Review of supercritical CO2 power cycle technology and current status of research and development. Nucl Eng Technol 2015;47:647–61. doi:10.1016/j.net.2015.06.009.

[20] Kritzer P, Dinjus E. An assessment of supercritical water oxidation (SCWO): Existing problems, possible solutions and new reactor concepts. Chem Eng J 2001;83:207–14. doi:10.1016/S1385-8947(00)00255-2.

[21] Dimitrov D, Zahariev A, Kovachev V, Wawryk R. Forced convective heat transfer to supercritical nitrogen in a vertical tube. Int J Heat Fluid Flow 1989;10:1988–90.

[22] Zhang P, Huang Y, Shen B, Wang RZ. Flow and heat transfer characteristics of supercritical nitrogen in a vertical mini-tube. Int J Therm Sci 2011;50:287–95. doi:10.1016/j.ijthermalsci.2010.06.014.

[23] Yamagata K, Nishikawa K, Hasegawa S, Fujii T, Yoshida S. Forced convective heat transfer to supercritical water flowing in tubes. Int J Heat Mass Transf 1972;15:2575–93. doi:10.1016/0017-9310(72)90148-2.

[24] Kim SH, Kim YI, Bae YY, Cho BH. Numerical Simulation of the Vertical Upward Flow of Water in a Heated Tube at Supercritical Pressure. 2004 Int. Congr. Adv. Nucl. power plants, Pittsburgh: American Nuclear Society; 2004, p. 1–6.

[25] Lei X, Li H, Yu S, Chen T. Numerical investigation on the mixed convection and heat transfer of supercritical water in horizontal tubes in the large specific heat region. Comput Fluids 2012;64:127–40. doi:10.1016/j.compfluid.2012.05.006.

[26] Zhang B, Shan J, Jiang J. Numerical analysis of supercritical water heat transfer in horizontal circular tube. Prog Nucl Energy 2010;52:678–84. doi:10.1016/j.pnucene.2010.03.006.

[27] Li ZH, Jiang PX, Zhao CR, Zhang Y. Experimental investigation of convection heat transfer of CO2 at supercritical pressures in a vertical circular tube. Exp Therm Fluid Sci 2010;34:1162–71. doi:10.1016/j.expthermflusci.2010.04.005.

[28] Launder BE, Spalding DB. The numerical computation of turbulent flows. Comput Methods Appl Mech Eng 1974;3:269–89. doi:10.1016/0045-7825(74)90029-2.

[29] Ansys. ANSYS Fluent Theory Guide 2013;15317:514. doi:10.1016/0140-3664(87)90311-2.

[30] E.W. Lemmon, M.L. Huber MOM. Reference Fluid Thermodynamic and Transport Properties, NIST Standard Reference Database 23 2007.

[31] Kim DE, Kim M-H. Experimental investigation of heat transfer in vertical upward and downward supercritical CO2 flow in a circular tube. Int J Heat Fluid Flow 2011;32:176–91. doi:10.1016/j.ijheatfluidflow.2010.09.001.

[32] Van Der Kraan M, Peeters MMW, Fernandez Cid M V., Woerlee GF, Veugelers WJT, Witkamp GJ. The influence of variable physical properties and buoyancy on heat exchanger design for near- and supercritical conditions. J Supercrit Fluids 2005;34:99–105. doi:10.1016/j.supflu.2004.10.007.

[33] Cheng X, Yang YH, Huang SF. A simplified method for heat transfer prediction of supercritical fluids in circular tubes. Ann Nucl Energy 2009;36:1120–8. doi:10.1016/j.anucene.2009.04.016.

[34] Cheng X, Schulenberg T, Koshizuka S, Oka Y, Souyri A. Thermal-Hydraulic Analysis of Supercritical Pressure Light Water Reactors 2002.

[35] Jackson JD, Cotton M a., Axcell BP. Studies of mixed convection in vertical tubes. Int J Heat Fluid Flow 1989;10:2–15. doi:10.1016/0142-727X(89)90049-0.

[36] Jiang PX, Zhang Y, Xu YJ, Shi RF. Experimental and numerical investigation of convection heat transfer of CO2 at supercritical pressures in a vertical tube at low Reynolds numbers. Int J Therm Sci 2008;47:998–1011. doi:10.1016/j.ijthermalsci.2007.08.003.

[37] Jones WP, Launder BE. The prediction of laminarization with a two-equation model of turbulence. Int J Heat Mass Transf 1972;15:301–14. doi:10.1016/0017-9310(72)90076-2.

[38] McEligot DM, Coon CW, Perkins HC. Relaminarization in tubes. Int J Heat Mass Transf 1970;13:431–3. doi:10.1016/0017-9310(70)90118-3.

List of Figures

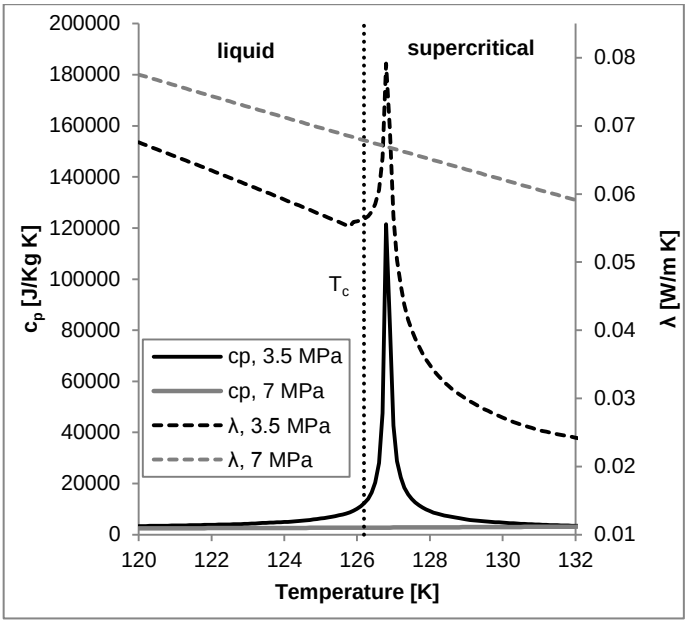

(a)

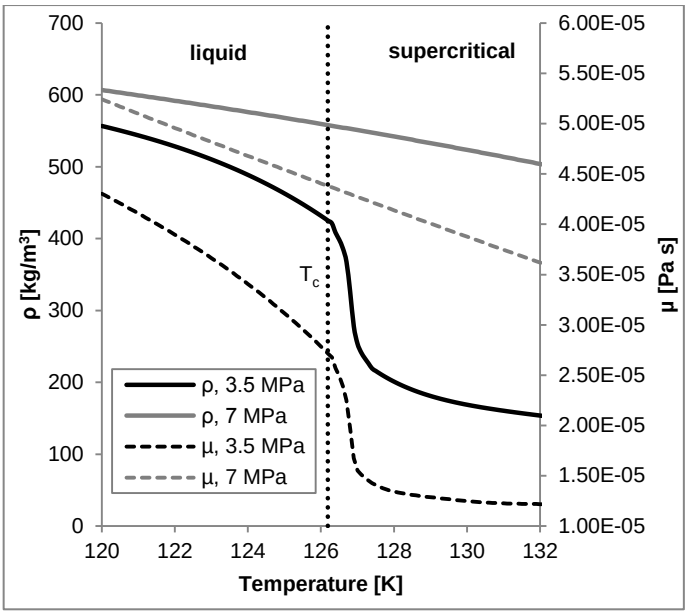

(b)

Fig. 1. Variation of thermophysical properties of nitrogen: (a) specific heat capacity and thermal conductivity, (b) density and viscosity.

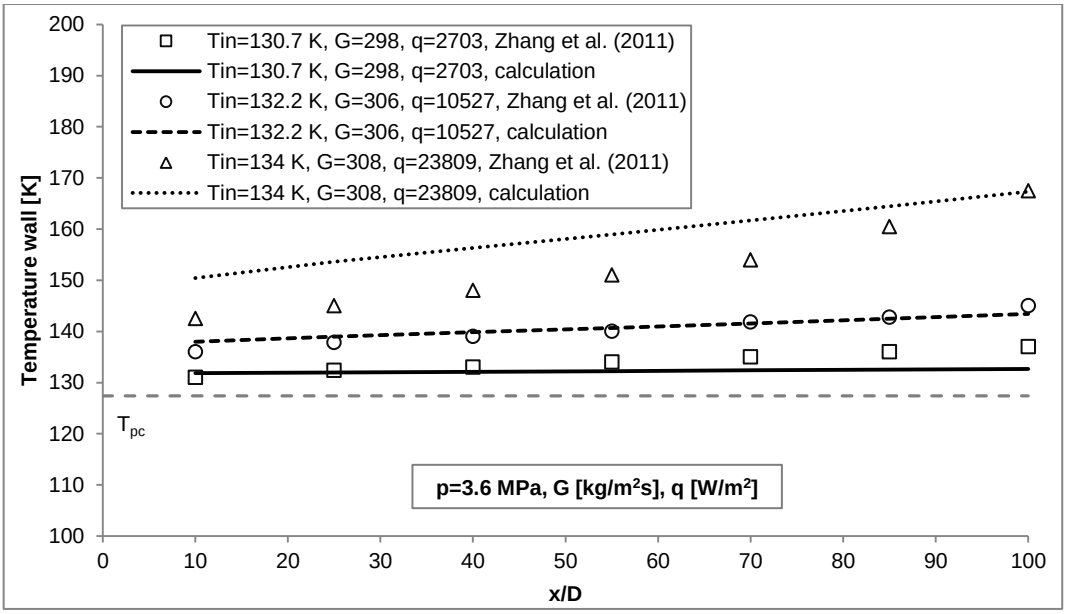

Fig. 2. Comparison of experimental and computed wall temperature as a function of position for supercritical nitrogen

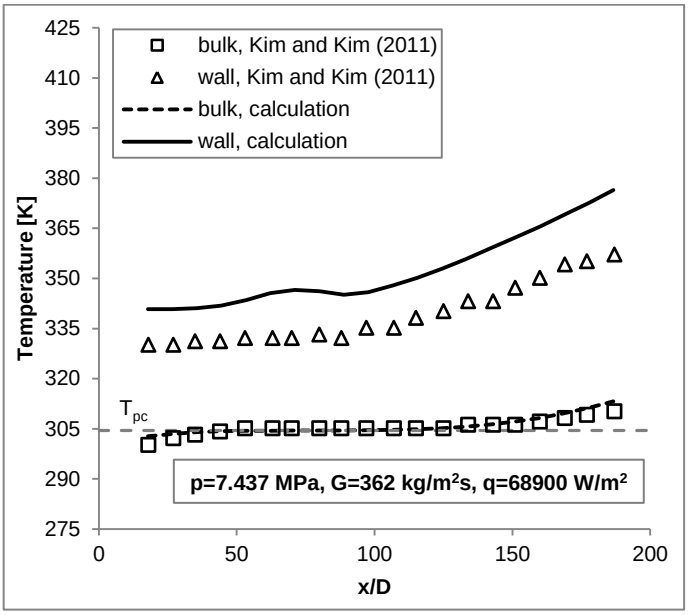

(a)

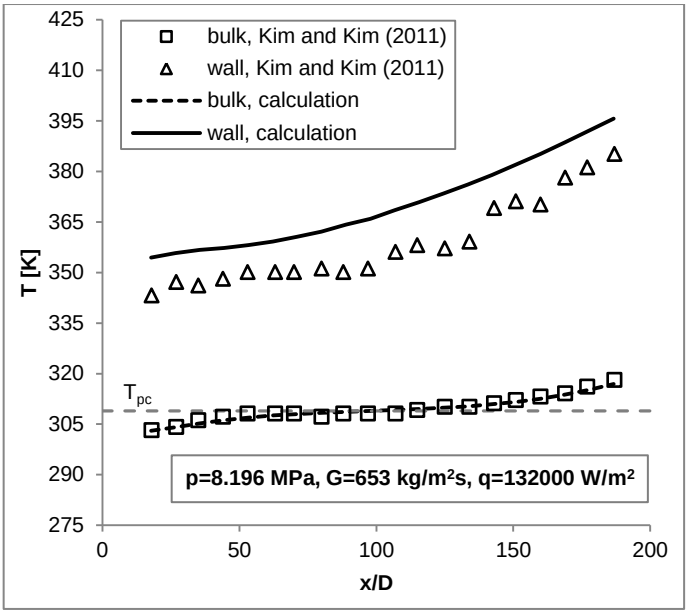

(b)

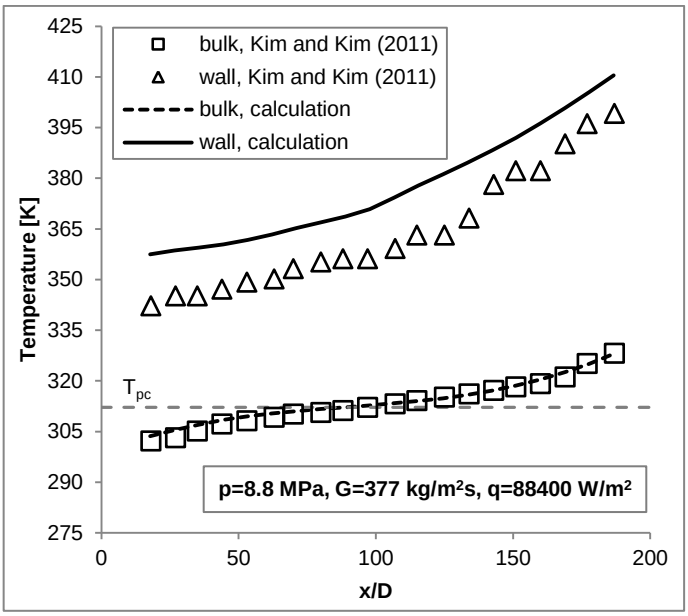

(c)

Fig. 3. Comparison of experimental and computed wall temperature as a function of position for supercritical CO_2

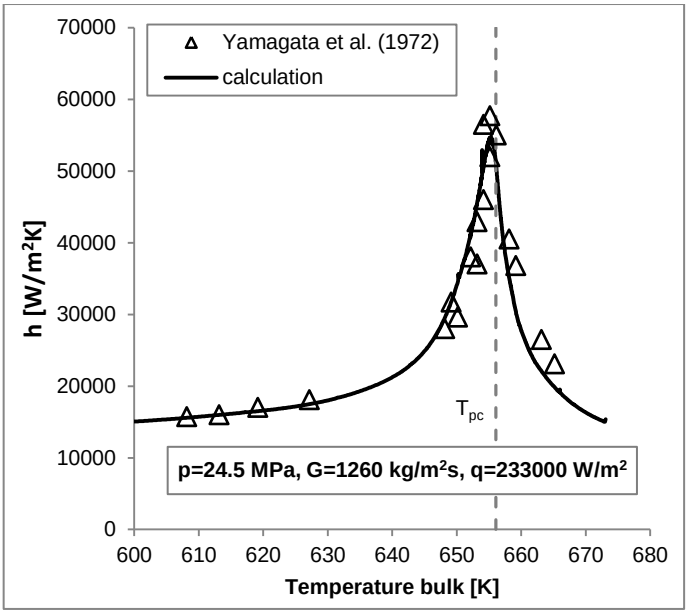

Fig. 4. Comparison of experimental and computed wall temperature as a function of position for supercritical water

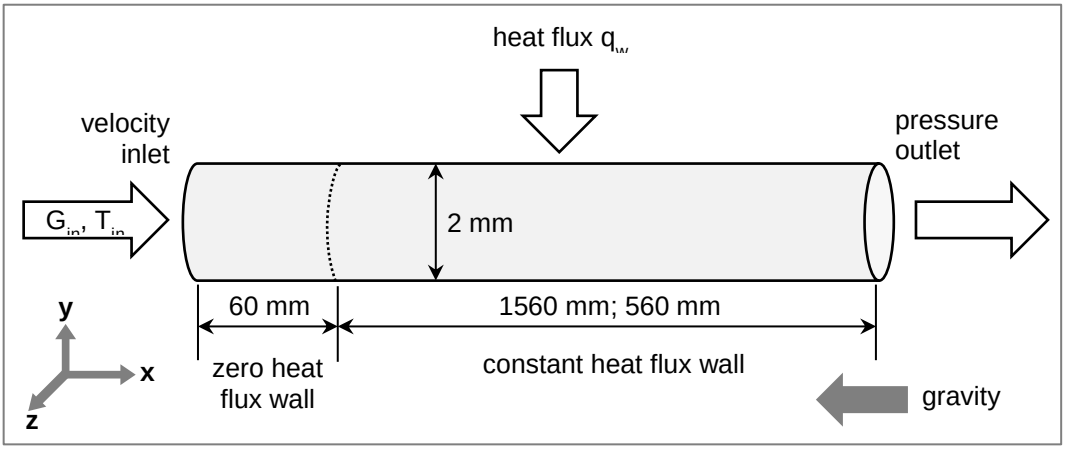

Fig. 5. Computational domain

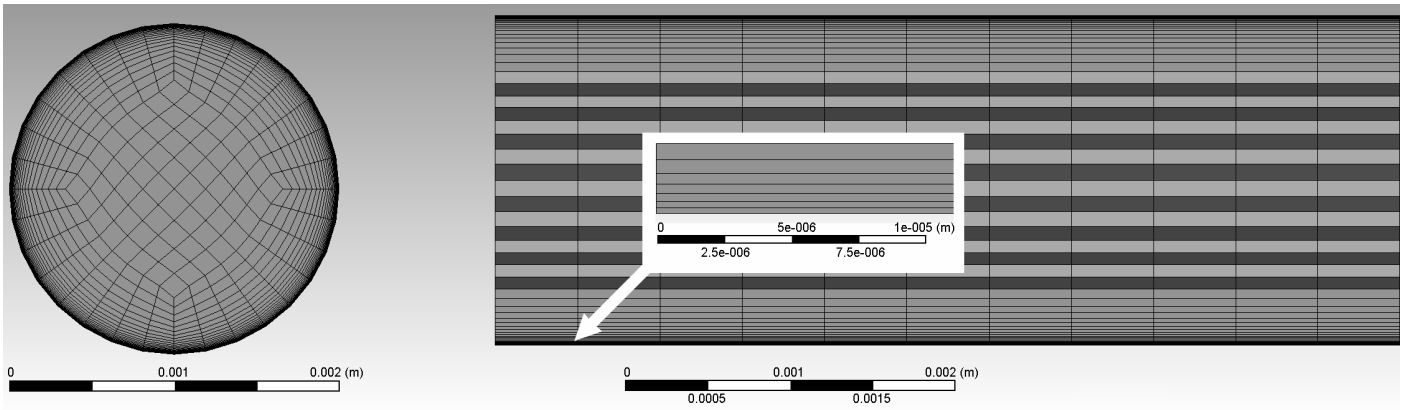

Fig. 6. Inlet and boundary layer mesh

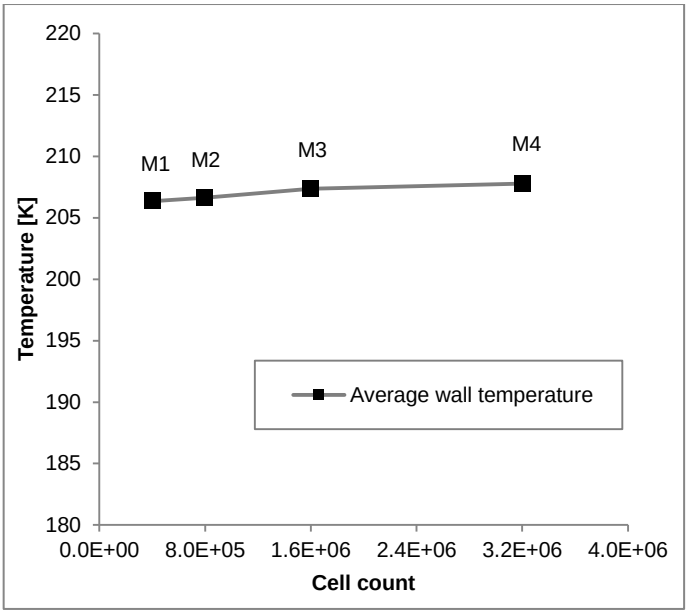

Fig. 7. Average wall temperature as a function of mesh density

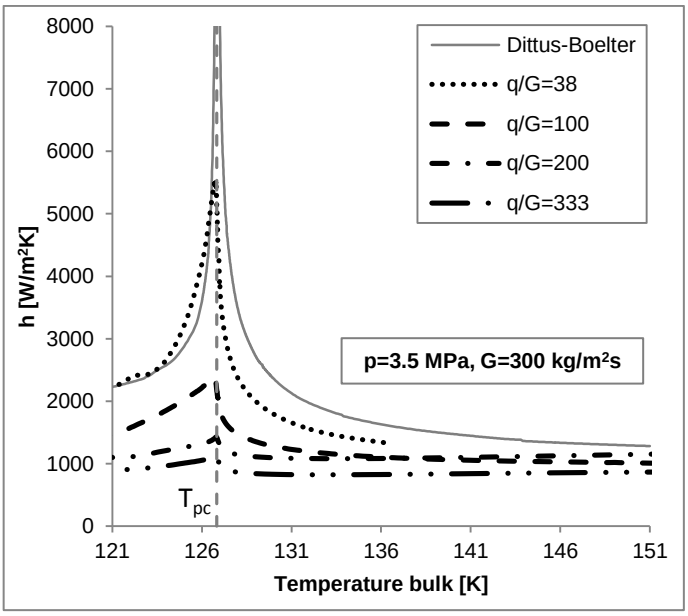

(a)

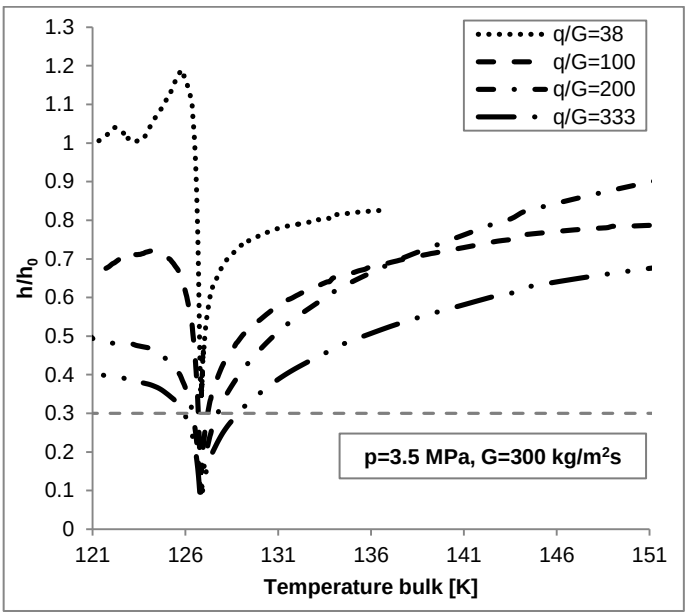

(b)

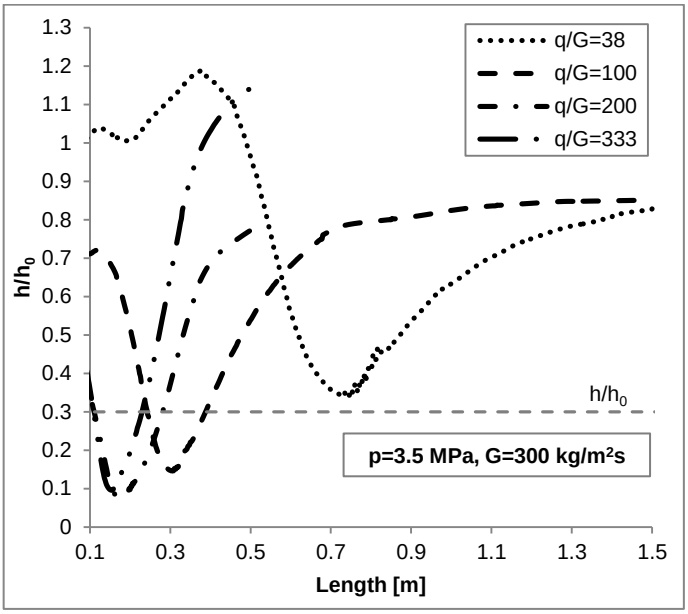

(c)

Fig. 8. Heat transfer performance in supercritical nitrogen P = 3.5 MPa, G = 300 kg/m^{2}s: (a) Local HTC as a function of bulk temperature, (b) ratio of HTC from simulation to HTC calculated with Dittus-Boelter correlation, (c) h/h_0 as a function of tube length

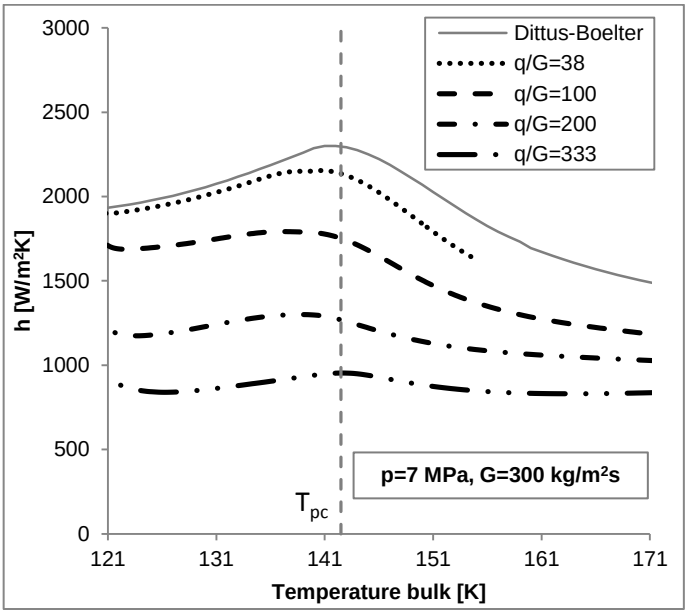

(a)

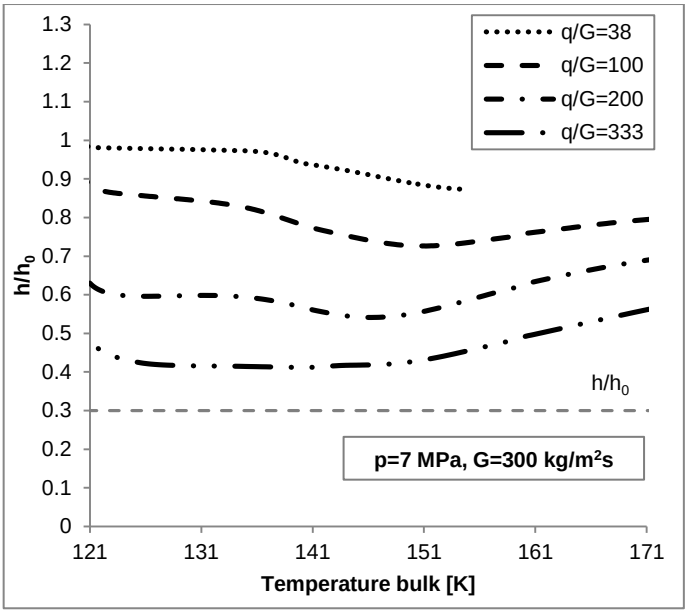

(b)

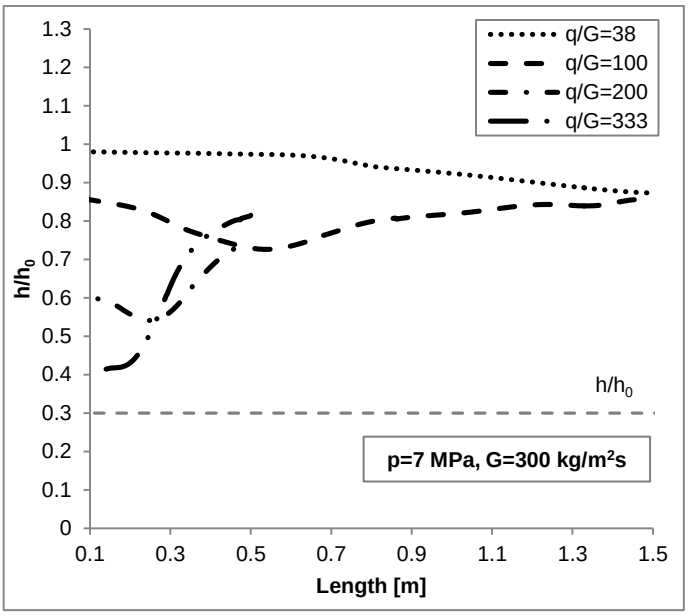

(c)

Fig. 9. Heat transfer performance in supercritical nitrogen P = 7 MPa, G = 300 kg/m^{2}s: (a) Local HTC as a function of bulk temperature, (b) ratio of HTC from simulation to HTC calculated with Dittus-Boelter correlation, (c) h/h_0 as a function of tube length

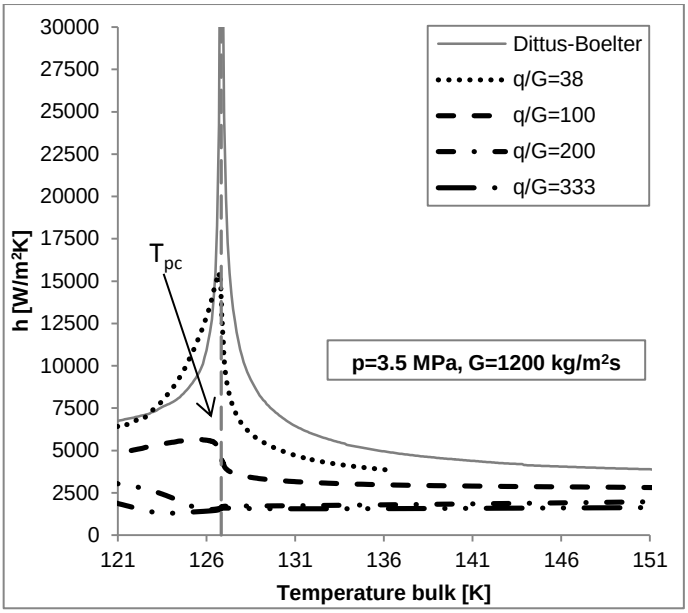
Dittus-Boelter
q/G=38
q/G=100
q/G=200
q/G=333
T_{pc}
p=3.5 MPa, G=1200 kg/m²s
h [W/m²K]
Temperature bulk [K]

(a)

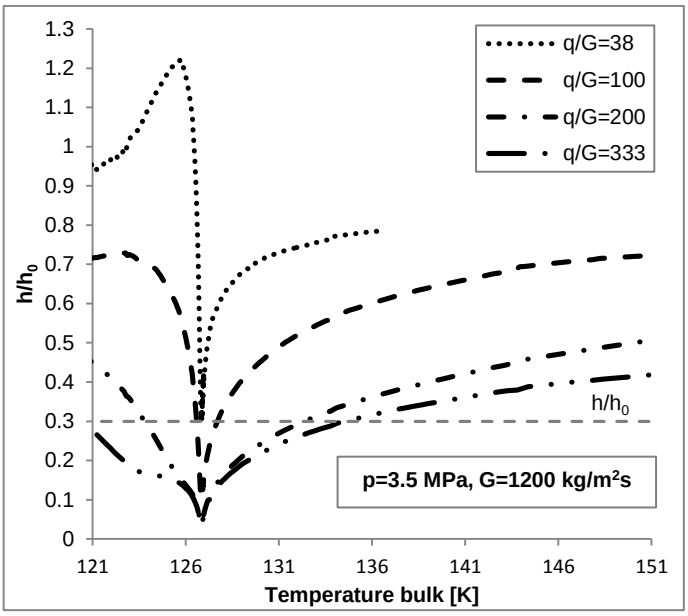
q/G=38
q/G=100
q/G=200
q/G=333
h/h0
p=3.5 MPa, G=1200 kg/m²s
Temperature bulk [K]

(b)

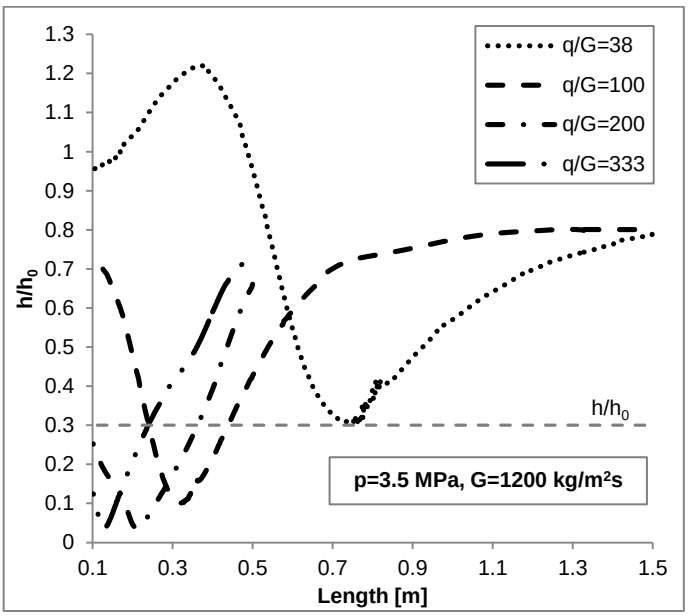
q/G=38
q/G=100
q/G=200
q/G=333
h/h0
p=3.5 MPa, G=1200 kg/m²s
Length [m]

(c)

Fig. 10. Heat transfer performance in supercritical nitrogen P = 3.5 MPa, G = 1200 kg/m^{2}s: (a) Local HTC as a function of bulk temperature, (b) ratio of HTC from simulation to HTC calculated with Dittus-Boelter correlation, (c) h/h_0 as a function of tube length

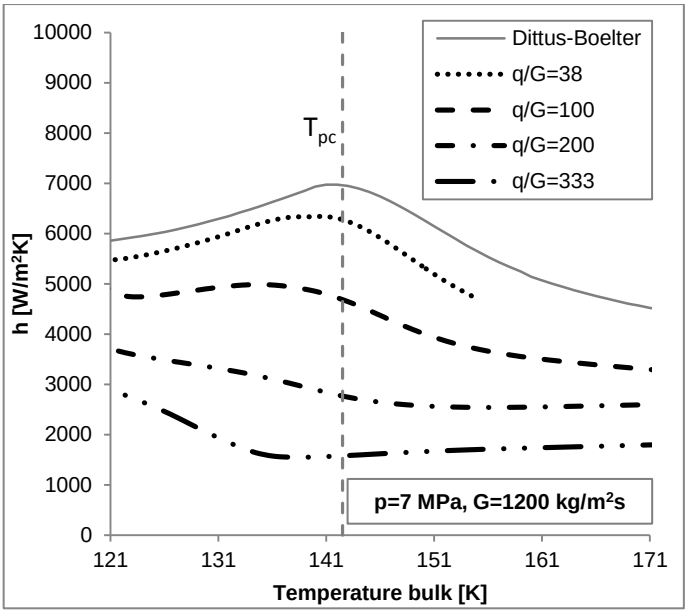

(a)

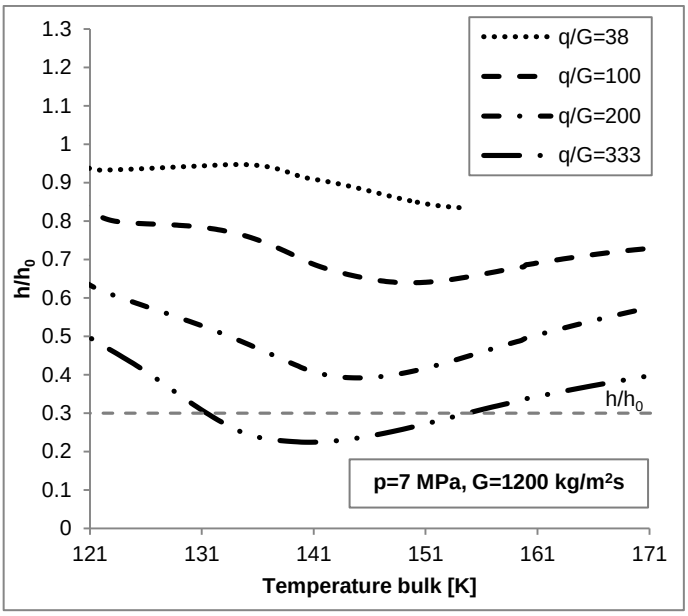

(b)

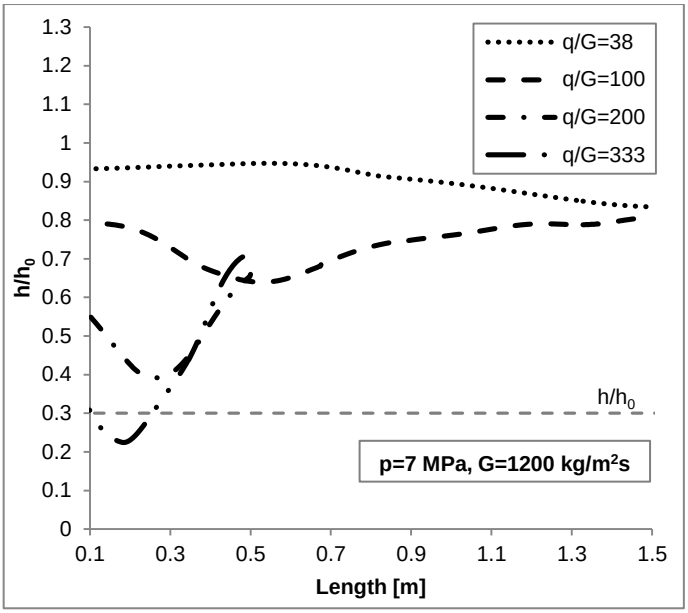

(c)

Fig. 11. Heat transfer performance in supercritical nitrogen P = 7 MPa, G = 1200 kg/m^{2}s: (a) Local HTC as a function of bulk temperature, (b) ratio of HTC from simulation to HTC calculated with Dittus-Boelter correlation, (c) h/h_0 as a function of tube length

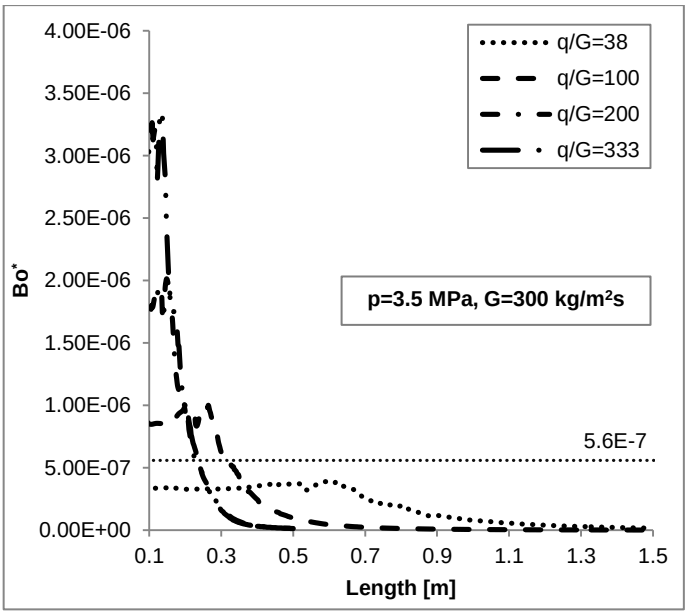

(a)

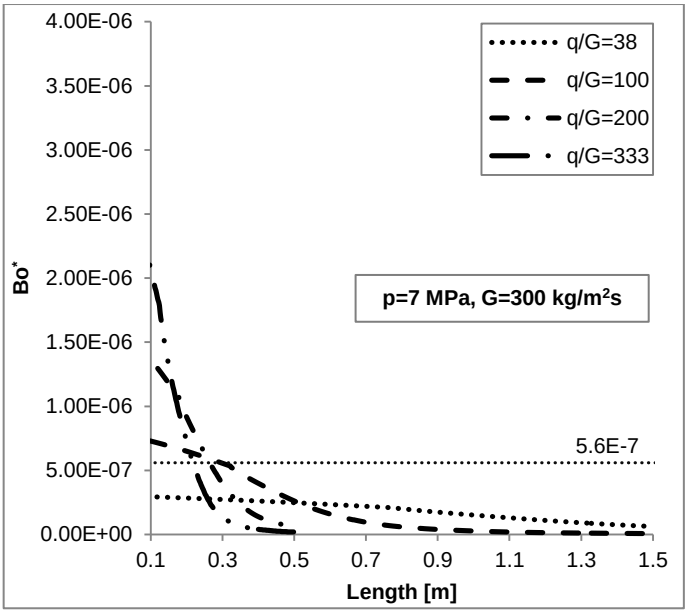

(b)

Fig. 12. Buoyancy parameter along the tube length: (a) P = 3.5 MPa, G = 300 kg/m^{2}s, (b) P = 7 MPa, G = 300 kg/m^{2}s

List of Tables

Table 1. Simulation matrix

Geometry	Flow orientation	Turbulence model	Working pressure p [MPa]	Inlet temperature T [K]	Mass flux G [kg/m^{2}s]	Heat flux q [W/m^2]
Tube D = 2 mm L =1560; 560 mm	vertically upward	standard k-ε enhanced wall treatment	3.5; 7	120	300; 1200	11 600 to 400000 q/G ≈ 38; 100; 200; 333